

## COMPUTATION OF ROUGHNESS AT SUBSTRATE COATING INTERFACE ON DEPOSITION OF ALUMINIUM OVER MEDIUM CARBON STEEL BY FRICTION SURFACING

D. K. SAHOO<sup>a,\*</sup>, B. S. MOHANTY<sup>b</sup>, R. ECHEMPATI<sup>c</sup>

<sup>a</sup>*Research Scholar, School of Mechanical Engineering, Sathyabama Institute of Science & Technology, Chennai, Tamil Nadu, India*

<sup>b</sup>*Professor, Dept. of Mechanical engineering, Sathyabama Institute of Science & Technology, Chennai, Tamil Nadu, India*

<sup>c</sup>*Professor, Dept. of Mechanical Engineering, Kettering University, Flint, USA*

Friction surfacing is happening to be a solid-state lining process, which proposes a mean of producing perfect coating between alike and unlike materials utilizing mechanical interlocking at the coating interface. During friction surfacing, the low rotational speed with high axial force normally produces good quality bonding; however, poor mechanical interlocking and cavitation at coating substrate interface resulted in an adverse effect on bond quality. In this present work, the substrate plate was preheated at three different temperatures of 100°C, 200°C and 300°C to create a coating of aluminium 6063 over EN8 medium carbon steel using friction surfacing. The mechanical interlocking was recognized from the specimen image of longitudinal cross-sectional slices, received from optical microscopy. Image recognition software (ImageJ) which depicts the substrate coating interface produce the interfacial roughness profile. The deepness of interlocking at coating interfacial region was monitored at different substrate preheating temperatures done by filter profile graph. The degree of interlocking has been calculated by interfacial roughness values of the profile graph by the use of Python programming language. Then this was compared with a bond strength to identify the relationship among them. Further push off and bonding strength caused by the dovetail shaped interlocking have become higher compared to narrow shaped interlocks stated by profile graph.

(Received March 30, 2020; Accepted May 25, 2020)

*Keywords:* Bond strength, Friction surfacing, FFT, Interfacial roughness, Push-off test, Substrate preheating

### 1. Introduction

Friction surfacing is a type of material bonding technology, which named as a corral of the friction stir welding joining procedure. [1] During friction surfacing, a downward axial force is applied on the spinning consumable rod, successfully subjected to relative transverse motion along the substrate materials to form a cladding. Generally, these surface alterations are brought down to the effect of corrosion and wear resistance of the substrate materials and to expose detailed material attributes, different as of the substrate matter. Over the last few years, a large number of papers have been published on the insight of the friction surfacing procedure and the interfacing of substrate adherence mechanism. Substance combination like stainless steel over low carbon steel [2] aluminium over aluminium [3] stainless steel over mild steel [4] substrate has been investigated continually compared to other materials. Normally the research concerning performance analysis, modelling of the work specimen, metallurgical analysis, corrosion behaviour and bond strength evaluation has been carried out for the obtained specimens.

---

\* Corresponding address: dillipkumarsahoo@gmail.com

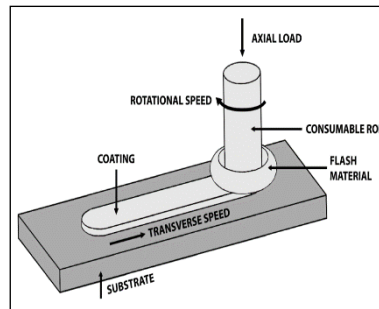


Fig. 1. The principle of friction surfacing.

Kumar et al.[5] inspected the relation between the process parametric relationship between aluminium alloy 6063 coated over the IS2062 Mild steel by friction surfacing and stated that when the value of coating width raised the coating thickness reduced. Besides, at highest torques, both the properties of coatings became superior. Stegmüller et al.[6] have introduced the inductive heating effect on the deposition of stainless steel over the aluminium substrate and quantified the production of flash mass on the influence of coating geometry. In their experimental work, Rafi et al. [7] analysed the microstructural features at the coating interface between mild steel and tool steel and inferred that proper cooling rate during friction surfacing has played a significant role for preventing carbide formation at the interface. Madhusudhan Reddy et al. [8] examined the wear resistance on the coating of titanium over aluminium metal matrix composites (AMMC) by friction surfacing and considerable improvements have been found out in the wear resistance of titanium alloy because of the interdiffusion of elements and the formation of a Nanocrystalline layer at the substrate coating interface. Hiroshi Tokisue et al.[9] investigated the effects of surface interference conditions and the mechanical properties between a single layer and a multi-layer deposition of 5052 aluminium alloy over 2017 aluminium alloy and found higher tensile strength on multilayer deposits than single layer deposits. Vilaca et al. [10] saw divergence relating the primary and the secondary flash mass creation on AISI 316 stainless steel cladding over HSS substrate as the FS process's outcome. In the comparison involving secondary and primary flash formation, Scanning Electron Microscopy (SEM) and Electron Backscatter Diffraction (EBSD) technique were used. FS process efficiency and the hardness of the deposition of AISI 316 stainless steel was more benefitted by Secondary flash formation. In their experimental work, Yoshinori katayama et al.[11] describes the various fundamental parametric combinations for deposition of AISI 316L austenitic stainless steel over AISI 440 martensitic stainless steel by FS process and suggested a more uniform deposition can be achieved at a lower rotational speed of the consumable rod. Gandra et al. [12] analysed the influence of FS mechanical behaviour like bending, tensile and wear characterization on the deposition of AA6082-T6 over AA2024-T3 substrate. The investigation of Pereira et al.[13] showed the wear characteristics of multi-layer coatings of AISI 1024, AISI 1045 and AISI H13 stainless steel over the mild steel substrate and the presence of martensite and bainitic microstructure at coating interface which induced to increase the hardness of the coatings was observed. On the subject of the deposition of AISI 316L over mild steel substrate, Puli et al. [14] did microscopy measurements at the coating interface and found huge stacking faults energy and high dislocation density associated during the FS process. The formation of low temperature during the FS process limited the formation of  $\delta$ -ferrite, which was found to make a great contribution for the enhancement of the anti-corrosion property of the FS coatings compared to manual metal arc welding. Amit Kumar Singh et al.[15] did the investigation of the Pitting corrosion resistance and the bond strength of stainless steel over the low alloy steel by FS process and also developed a predictive model by correlating input variables and the process response which could design new friction surfacing applications. Govardhan et al. [16] indicated the potential application of FS in petrochemical and chemical industries, because of corrosion analysis on austenitic stainless steel accumulated on mild steel. Rao et al.[17] have performed a broad study on the creation of friction surfaced coatings for different nonferrous substrates and found very fine grain microstructures with better mechanical

properties compared to the original material. Kumar et al. [18] analysed the correlation among the process parameters and coating geometry of AA 6063 aluminium alloy over IS 2062 medium carbon steel and observed a decrease in the coating thickness following an increase in the width of the coating and the width and thickness of the coatings having higher values at lower and higher torque conditions respectively. Stefanie et al. [19] made an experimental study of the development of microstructural and dynamic recrystallization at the coating interface of a nickel-based alloy 625 using friction surfacing and saw a palpable effect of the particle nucleation on which there was a highly significant effect from localized shear stress and residual strain produced during the process. George Nixon, et al. [20] studied the interfacial characteristics of the deposition between AISI316 stainless steel and EN24 medium carbon steel substrate and found the absence of carbide particles at the coating interface which increased the productivity of good bonding. Samuel Silverio et al. [21] took up the performance and geometrical analysis on friction-surfaced coating between AA5083-H112 on AA2024-T3 for their study and concluded that the development of heat and plastic deformation had catalysed the dynamic recrystallization of the consumable rod. Juan Carlos et al. [22] have assessed the process control parametric combinations between aluminium 6351 and aluminium 5052 by the use of the double-layer friction surfaced deposition process. Hongjun Li et al. [23] analyzed the microstructural behaviour on friction surface deposition of aluminium alloy 5983 over DH36 steel and confirmed the elemental diffusion of Fe and the presence of FeAl<sub>3</sub> intermetallic compounds at the coating interface. Seyedeh Marjan Bararpour et al.[24] dealt with the thermomechanical performance using ABACUS software on the deposition between AA5083 over AA5052 using friction surfacing and claimed a change in grain structure at the coating interface as not greatly influenced by strain energy present during the coating.

This work is related to the quantification of the roughness at the coating interface on the deposition of aluminium 6063 into medium carbon steel using the FS process. Interfacial roughness profile was prepared using ImageJ software which deals with the coating substrate interface. Python programming language was used for the calculation of the degree of interlocking and compared with bond strength for the identification of the relationship among them. Microhardness and push off test were also conducted to enable an analysis of the bonding mechanism. A scrutiny of the recent state of the art of this subject illustrates that until now no work has been carried out for this type of interfacial roughness calculation with this material amalgamation. Therefore, the originality of contemporary study is precisely explained.

## 2. Materials and methods

For the coating material, precipitated hardening aluminium alloy AA6063 has been used, provides superior strength and high corrosion resistance properties. A rotating rod with a diameter of 18 mm cut into a 100 mm length was employed for the experiments. The wrought substrate material EN8 (C0.42Mn0.5Si0.24) with a dimension of 150x100x6 mm was utilized in the testing which offered artificial ageing properties due to the precipitation hardening effect of MnSi partition. In Tables 1 and 2, the details of the chemical composition of the as-received EN8 carbon steel and AA6061 material are summarized respectively.

*Table 1. Chemical Composition of EN8 Medium carbon Steel.*

Material	C	Mn	P	S	Si	Ni	Fe
% of composition	0.36	0.60	0.05	0.05	0.10	0.01	Balance

*Table 2. Chemical Composition of AA 6063 Aluminium Alloy.*

Material	Mg	Si	Cr	Mn	Ti	Zn	Fe	Al
% of composition	0.55	0.4	0.1	0.1	0.1	0.1	0.35	Balance

A custom-made vertical milling machine has taken for the procedure of friction surfacing which employs the downward axial force onto the spinning consumable rod utilizing a pneumatic cylinder. The heat supply for the substrate plate was an inductive power unit (2kW) and a regulator used for the regulation of the substrate plate temperature to achieve 100°C, 200°C and 300°C. Before initiation of the coating, all the materials were scoured to eliminate any kind of contamination. The evaluating properties of both the coating and substrate materials were recorded earlier and after the friction surfacing. Design of experiments was developed using the value of fundamental the parameters of friction surfacing like the rotational speed (1500, 3000 rpm) axial force (4, 6 kN) and constant transverse speed (150 mm/min). Three separate specimens were produced for each parametric combination to ensure achievement of a high statistical significance. Details are displayed in table 3. The specimens obtained from different parametric combinations were shown in figure 2.

Using Vicker's hardness test machine, the hardness value of both substrate and mechtrode were computed earlier and later friction surfacing. Up to eight indentations were marked on the substrate near coating, coating interface and coating region to measure hardness value. An inter indentation distance of 0.3 mm on medium carbon steel and 0.6 mm on aluminium was regarded as suitable for the precluding the impact of strain hardening effect arising as a consequence of the nearby indentation,

Khalid et al.[25] and Voutchkov et al.[26] recommended the bond strength for the coating was ascertained by performing push off and bending tests together respectively. For conducting the push-off test, the specimen was crushed to a cylindrical shape and initiation of whole started from the back of the substrate material through which the coating was pushed off through the use of a pin. In a universal testing machine, the specimen was instated with a 3-point bend fixture for conducting bend test. The specimen standard was fixed between two supporting blocks and increasing the load gradually to the specimen until the breakage occurs in the specimen.

*Table 3. Parametric combination of the friction surfacing.*

Sample No	Axial Force (kN)	Rotational Speed (rpm)	Substrate temperature(°C)
S1	4	1500	100
S2	4	1500	200
S3	4	1500	300
S4	4	3000	100
S5	4	3000	200
S6	4	3000	300
S7	6	1500	100
S8	6	1500	200
S9	6	1500	300
S10	6	3000	100
S11	6	3000	200
S12	6	3000	300

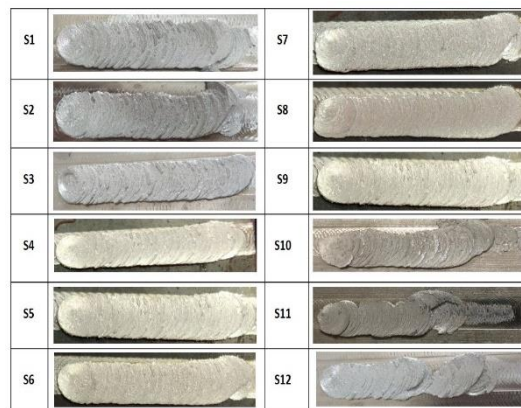


Fig. 2. Specimen obtained from different parametric combinations.

### 3. Establishment of the interfacial roughness value

In this present work, the author prepared a specimen cross-section, which revealed the bonding between coating and substrate to an assured degree of mechanical interlocking. During the initial investigation, the quality of the bonding was seen having an influence on the geometry of intermixing at the interface; which could be presented in sequence by the height and the distance of the peak noticeable at the interface. The profile obtained possibly will be benchmarked by a roughness profile originated as of surface topography.

An image recognition software (ImageJ) had used for the calculation of the interfacial roughness profile graph for the specimen coating-substrate and then there is an estimation of height and distance of the profile peaks by using the specific value obtained from the roughness profile. In the end, the readings were examined with the mechanical bond strength to establish any feasible correlation between interfacial roughness and bond strength.

The image recognition software tool ImageJ is used for the manipulation of images of the specimen cross-sections and details are shown in Figure 3. Thus, a graph was generated of which X and Y coordinate values were filled into a range of the array. Those obtained values were then refined using a specific program that was performed by the Python. It was operated at a specified spatial gap as well as the series of length in direction of the lengthwise cross-section.

#### 3.2. Stages involved for data processing in Image

Stage I. The cross-sectional image was introduced into the image recognition software tool as Tagged Image Format (TIF) and by applying scale function, the constituent pixel was converted into the required dimensional coordinates (mm was selected).

Stage II. An 8-bit scale image is formed by the tagged formatted image from the coating interface line. The coating interface line was obtained by the application of the image edge option. (A discontinuous interfacial line may found at some location where the plugin could not detect an edge, due to the lack of contrast between adjacent grey values).

Stage III. The binary converted image that contains black (value 255), white (value 0), and authorized the use of analysis of a line graph tool. The algorithm acknowledges the black pixels and X-Y Cartesian system is allocated by each pixel a coordinate. (During the position of the undercut, only the size of the vertical dimension (thickness of the coating) and shape of an undercut could not be considered for successive evaluation. The tool on the location where there was a discontinuous interfacial line employed linear interpolation).

Stage IV. The values range of X-Y coordinates were obtained, saved into a .txt file, and apt for extended processing in the python shell. The accurateness in the identification of interface was reliant purely on the quality of the image.

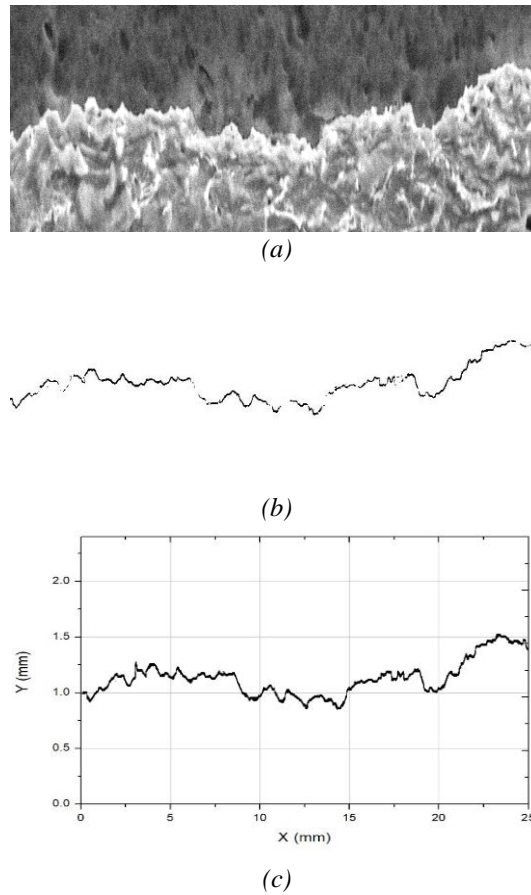


*Fig. 3. Utilization of the lengthwise cross-section and its flow chart: (a) longitudinal cross-section with an 8-bit greyscale image, (b) drawing of the coating-substrate interface, (c) generation of a graph.*

The roughness profile observed in a time domain can be seen as an assortment of sinusoidal functions with different wavelengths and amplitudes. The measured object will be strained with various wavelengths to achieve data on different matters. For a given surface, the comprehensive geometrical form, which provides a longer wavelength, may not be devoted to the surface roughness readings [27]. Hence, the primary profile obtained was split towards ‘form’, ‘waviness’, and ‘roughness’ profiles which were attained by the employment of Fourier transformation and were dependent on the associated wavelengths.

### **3.3. Stages involved in the development of python code**

The following are the basis of the requisite stage on which the partition of two superimposed triangular functions of dissimilar amplitudes (0.75 and 0.25 mm) and wavelengths (1.5 and 0.5 mm). A unique development of a primary profile filtering process and a flow chart of the python code are displayed in Fig. 4.

Stage I. Import the .txt file formed by ImageJ to the python shell and separated by two ranges of arrays. One array holds all distance and width of profile peak values plotted in the X direction and all values of the amplitude of the profile peaks were plotted in the Y direction.

Stage II. After the partition, the value size on the X-axis and its sampling frequency is determined by the spacing between the single point data and values saved in another array. All duplicate values (undercut section) are deleted resulting in a sequence of X values with a defined step size of 0.0068 mm.

Stage III. The Fast Fourier Transformation (FFT) is performed using Equation 1. Using the FFT, the profile is sifted renouncing a certain frequency interval and eliminating distinct higher and lower frequencies.

$$f(x) = s(x) = \frac{a_0}{2} + \sum_{k=1}^{\infty} (a_k \cos kx + b_k \sin kx) \quad (1)$$

Stage IV. An inverse FFT python program was performed and used to evaluate the filtered Values of the data. Using the profile curve the mean Y values are calculated and subtracted from each single Y value for the removal of the profile upset from the zero in the X-axis. Calculation of the specific roughness is done for quantification of the dimensional size of the peaks and valleys.

Stage V. The Y-axis values of the main profile transferred to the FFT domain are characterized by amplitudes and their associated decreasing wavelength. The mean value of all amplitudes (Y values) are represented by the coefficient  $a_0$  and as the initial value of the FFT array. The mean of the roughness profile is shifted to zero when the value  $a_0$  is subtracted from the profile Y-values, which indicates its congruence to the X-axis.

A filtering process was used for the elimination of the specific wavelength which was employed a zero multiplier to specific amplitudes. A bandpass filter was used for scripting the wavelengths between certain values (0.1 to 1 mm). This indicated the wavelength entries falling among those values have been entered in a discrete indexed array. The bandpass range of array was developed using the index array that illustrates a "1" at each access of the wavelength to be surpassed. All unwanted amplitudes were removed by multiplying the bandpass array with that of the FFT array. The created array is a complex number with both real and imaginary parts, which connected with the decreased wavelength. The overall amplitudes of FFT were analyzed by finding the sum of sines and cosine values in geometrically.

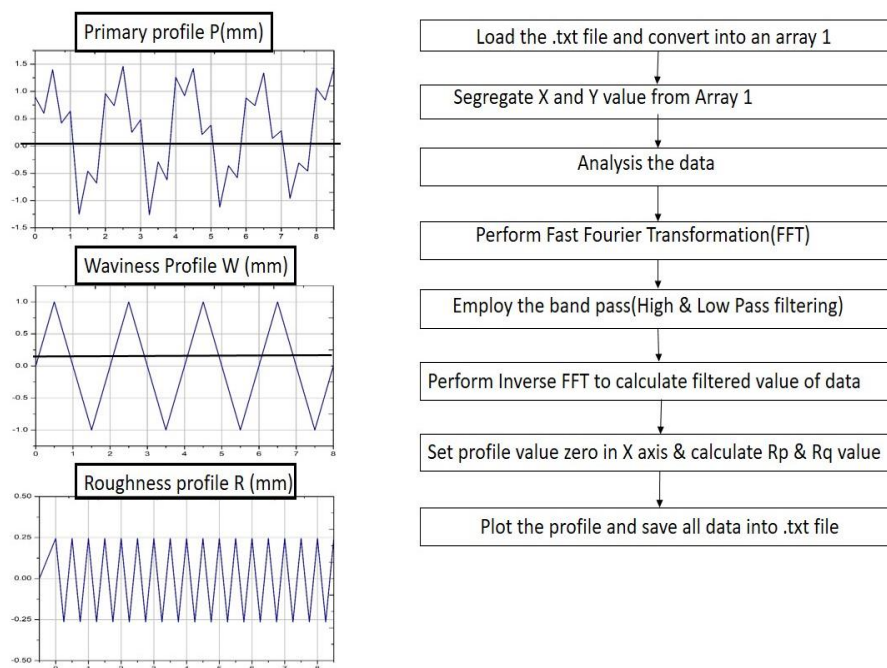


Fig. 4. Diagrammatic demonstration of the main profile filtering process: partition of the primary profile (P) to waviness (W) and roughness (R) profiles based on two superimposed triangular functions.

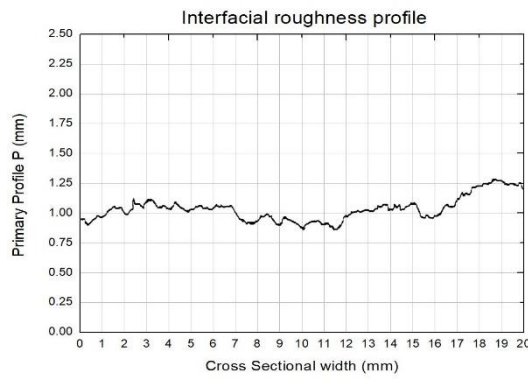


Fig. 5. Fundamental standard of the filtering procedure: acquired primary profile.

The initial value of the FFT range must be real numbered and the values were transferred to the roughness/distance domain by applying IFFT, which explained a filtered profile in Fig. 6. The different roughness attributes (named R with a related alphabet) can estimate from the filtered value. The arithmetic mean of absolute values computed from the mean line is known as average roughness (Ra) as the X-axis shown in Fig. 7.

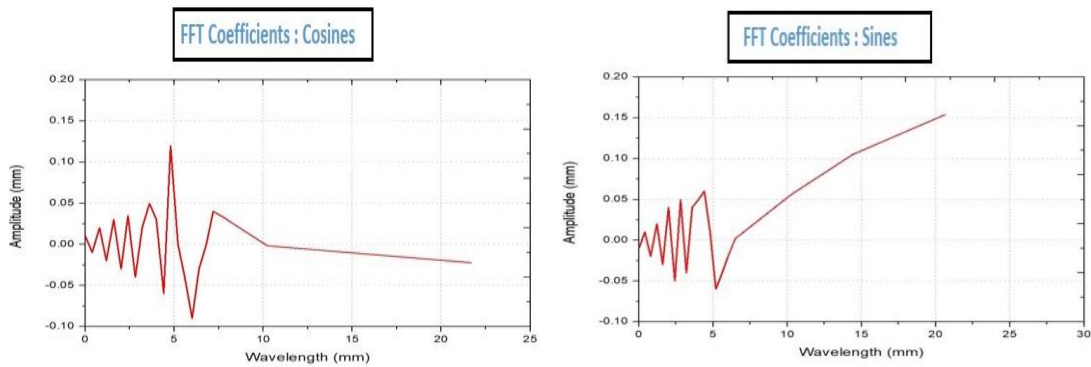


Fig. 6. Fundamentals of the filtering procedure: FFT with the corresponding complex-valued arrays multiplied with a band-pass filter array containing both "0" and "1" values.

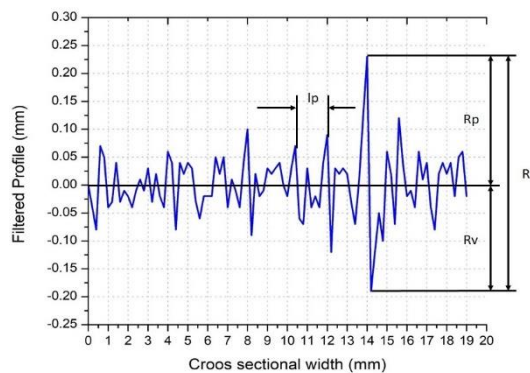


Fig. 7. The fundamental principle of the filtering method: filtered roughness profile following carrying out IFFT.

$$R_a = \frac{1}{n} \sum_{i=1}^n |r(i)| \tag{2}$$

Rq expresses the root-mean-square value:

$$R_q = \sqrt{\frac{1}{n} \sum_{i=1}^n (r(i))^2} \quad (3)$$

The peaks of the filtered value ( $R_p$ ) and valleys of the same ( $R_v$ ) of the profile can be explained by an ‘overall’ or ‘local’ value. ‘Local’ signifies the slope of the graph as positive next to the peak value on the single region and another value is negative, at the same time the ‘overall’ values allot the extreme peak-to-valley values there for the whole graph:

$$R_p = \max \textcircled{\text{R}} \quad (4)$$

$$R_v = \left| \min \textcircled{\text{R}} \right| \quad (5)$$

The summation of the total highest peak and the absolute value of the deepest valley is called as the absolute height of the profile ( $R_t$ ), which is described by:

$$R_t = R_p + R_v \quad (6)$$

It was regarded that the density of the mechanical interlocks along the coating length can be probably a significant bonding attribute, which is stated by the mean, distance  $l_p$  in between local maxima in the roughness profile, So:

$$l_p = \frac{1}{n} \sum_{i=0}^n (X(R_{p|i+1}) - X(R_{p|i})) \quad (7)$$

## 4. Results and discussion

### 4.1. Mechanical bond strength

Mechanical bond strength found by conducting a push-off test to measure at which rate coatings were detached from the substrate. The maximum load observed is essential to break the bond was separated by the notified fractured area for the determination of the coating bond strength. During the testing, the maximum values had generated through the tests suggesting an obvious relationship between bond strength and fractured area. Smoothness at the coating interface resulted in lower roughness values, which reduced the value of push-off strength. Increase in the temperature of EN8 carbon steel substrate during FS process allowed the work hardening of consumable aluminium material resulted in increases the yield strength of the coating. At the substrate temperature 100°C, at low process parametric combination of axial force (4 kN) and rotational speed (1500 rpm) cavitation was visible at the interface showing poor bonding strength (43Mpa). The bonding strength increased to 51Mpa for process parametric combination (Axial force 4 kN, rotational speed 1500 rpm) when the substrate temperature was increased to 300°C resulting in an increase in roughness at the interface.

Parametric combination of high axial force (6 kN) and low rotational speed (1500 rpm) at substrate temperature 300°C provides high push-off strength values (92 Mpa) since can be observed from Figure 8. Higher combination of rotational speed (3000 rpm) and axial force (6kN)

at increased substrate temperature offering poor push-off strength due to artificial ageing of aluminium which promotes the development of segregation from substrate materials.

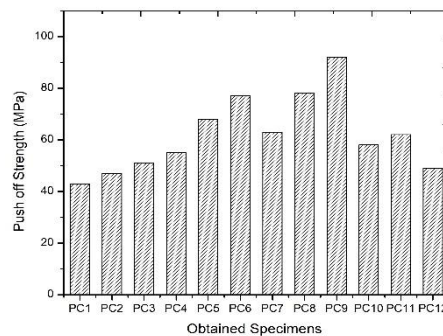


Fig. 8. Comparison of push-off strength values of all parametric combinations.

#### 4.2. Metallurgical investigation

Samples obtained in longitudinal cross sections by slashing the samples from the middle sectional plane for making the interfacial roughness profile graph details. Figure 9 relates to the interfacial roughness profile graph of various samples obtained from different parametric grouping. A 7 mm long along the coating direction had taken and arranged for interfacial roughness analysis for all the samples. The interfacial roughness value estimated through the calculation of the roughness values for three dissimilar profile types namely smoothed courser and waviness. Each profile type is being formed by deploying three profile filters with three different wavelength values shown in Fig. 4.

The smoothed roughness description had established by neglecting all the outside wavelengths ranging from 0.1 to 1 mm. A courser roughness profile generated by filtering the wavelength at a range from 0.5 to 4 mm. The waviness roughness profile was attained from the filtering wavelength ranging from 2 to 8 mm. The profile graph showed the presence of a minute difference in roughness parameters for both smoothed and waviness profiles for different combinations of the coating input parameters and therefore not regarded for extra exploration. The courser roughness profile was employed for investigating the coating interfacial roughness for all the samples obtained (Figure 9). The figure shows the specimen obtained from lower combinations of axial force and rotational speed (4kN, 1500 rpm) providing a cross-section having more pores and cavities at the interface offering finer roughness profile which indicated poor mechanical interlocking. Increase in the substrate temperature allows the mechtrode aluminium material to work-hardened and as a result minimizing the number of cavities and pores at the interface that increases the roughness values. Too high substrate temperature makes the thicker viscoplastic material transformation from aluminium creating an adverse effect during the deposition process. At high of axial force (6kN), there was an increase in the dimension of mechanical interlocking with the minimum number of cavities providing a higher roughness value. Increase in the rotational speed at constant axial force caused the development of a thinner distribution of aluminium over steel substrate, which made poor mechanical interlocking at the interface, as increasing the axial force at steady rotational speed retains the capability to coat the cavitations existing during the coating with mechtrode materials. Normally the cavitations are most likely to occur during coating when the specimen is experienced at low axial force.

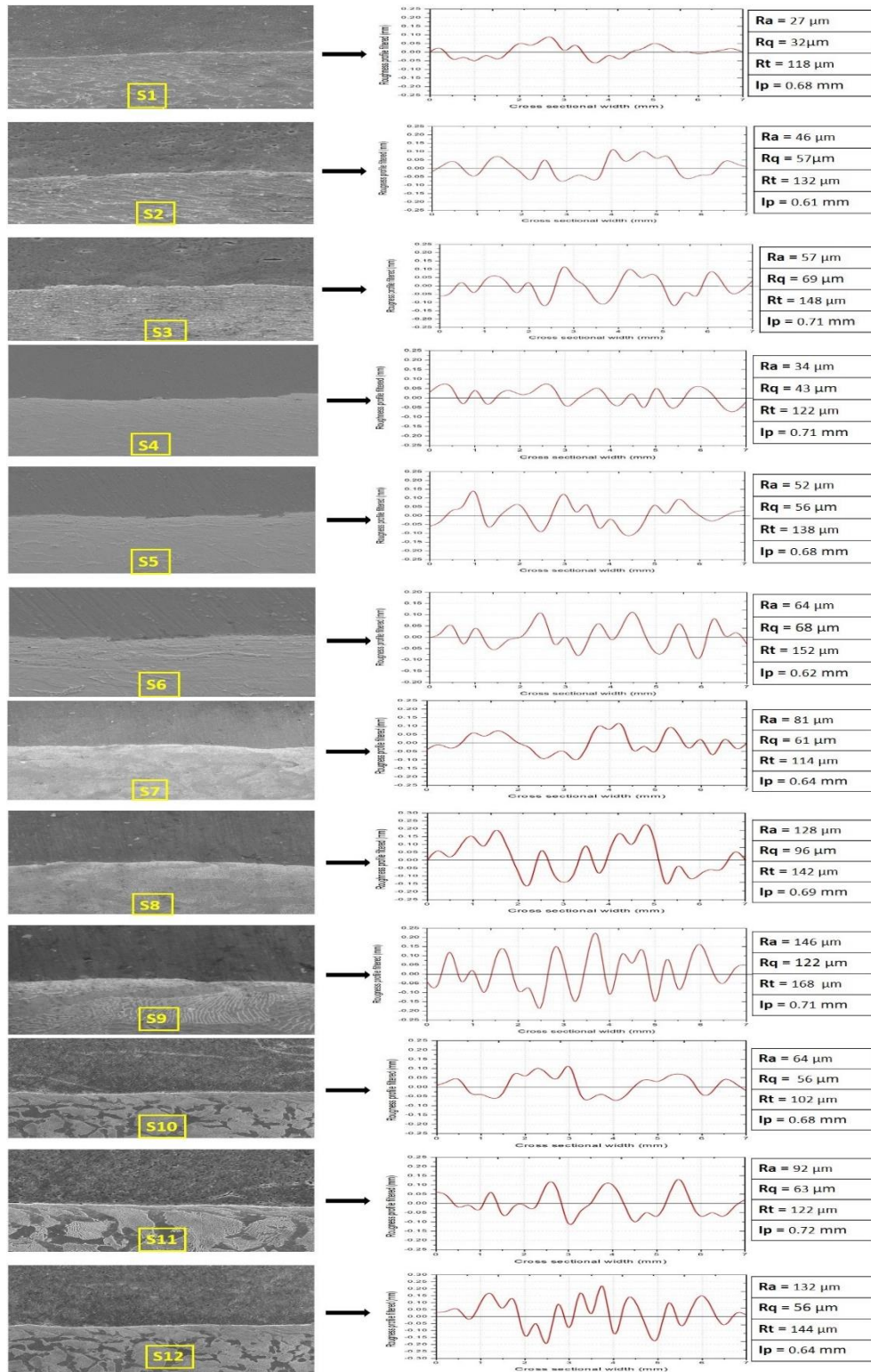


Fig. 9. Roughness profile of samples obtained from all parametric combinations filtering wavelengths between 0.5 and 4 mm.

Fig. 10 represents the development of Ra concerning various process parameters of friction surfacing. It can be seen that the Ra values were higher at higher axial force and increases with increase in substrate temperature. The amplitude of Ra values was marginally changed for the

rotational speed of the mechtrode. The behaviour of the Rq is almost similar to Ra, which has been confirmed from Fig. 11.

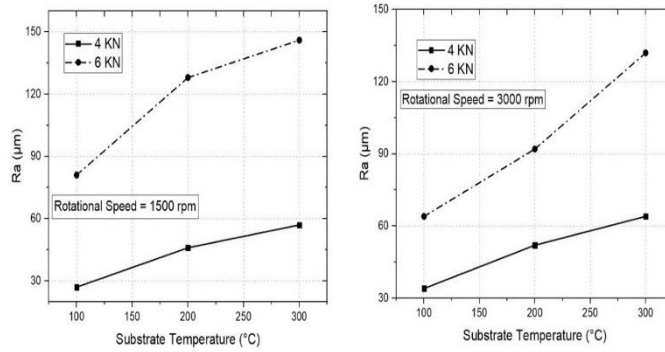


Fig. 10. Effect of Ra on rotational speed and axial force at different substrate temperature

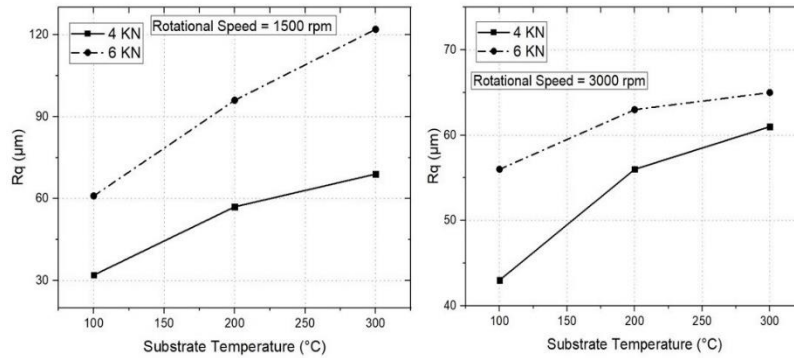


Fig. 11. Effect of Rq on rotational speed and axial force at different substrate temperature.

The high bonding integrity was achieved at the rotational speed 1500 rpm, axial force 6kN with a substrate temperature of 300°C. Those samples illustrated the development of undercuts, which were loaded fully with mechtrode materials. There was variation in the structure of mechanical interlocking compared to dovetail and taper shaped profile. The dovetail shaped profile (Fig. 12a) provides high push-off strength whereas the taper shaped profile (Fig. 12b) provide poor push-off strength. The coating interfacial profile including mechanical interlocking, push-off strength, roughness figures seemed to highly influence by the process parameters like rotational speed and axial force.

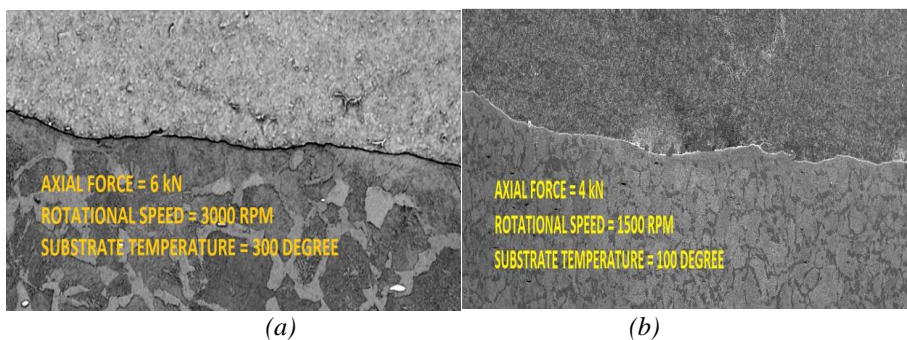


Fig. 12. Longitudinal cross-sections for (a) highest (b) lowest extreme values of rotational speed, axial force and substrate temperature.

## 5. Conclusions

1. Variation in the coating substrate interfacial topology was well presented through the unique approach of developing an interfacial roughness profile. The coating material transformation between the substrate and mechtrode material was discovered by filtering the primary roughness profile at a wavelenghts range from 0.5 to 4 mm.

2. Concerning the push-off strength, bonding quality (92MPa) obtained from the process parametric combination of axial force 6 kN, rotational speed 1500 rpm, transverse peed 150 mm/min and substrate temperature 300°C was seen to be good. Roughness value achieved from these parametric combinations was large.

3. Mixed-mode failures occurred at all push-off specimens i.e. both at substrate coating interfacial zone and the aluminium deposition zone.

4. Variation in the mechanical interlocking was seen based on the dimension and shape. Dovetail shape profiles produced high push-off strength values, at the same time tapper shaped profile appeared in low push-off strength values. A particular shape might not be obtained through the interfacial roughness profile from the current technique employed in the study, which will be taken into account as future work.

## References

- [1] H. Klopstock, A. R. Neelands: U.K. Patent 572789, 1994.
- [2] D. Govardhan, K. Sammaiah, K. G. K Murthi, G. Madhusudhan Reddy, *Materials Today Proceedings* **2**(4-5), 3511 (2015).
- [3] H. Krohn, S. Hanke, M. Beyer, J. F. Dos Santos, *Manufacturing Letters* **5**, 17 (2015)
- [4] R. George Sahaya Nixon, B. S. Mohanty, R. Sathish, *Defence Technology* **4**(4), 306 (2018).
- [5] B. V. Kumar, G. M. Reddy, T. Mohandas, *Defence Technology* **11**, 275 (2015)
- [6] M. G. R. Stegmuller, P. Schindele, R. J. Grant, *Journal of Materials Processing Technology* **216**, 430 (2015).
- [7] H. K. Rafi, G. D. J. Ram, G. Phanikumar, K. P. Rao, *Mater Des.* **32**, 82 (2011).
- [8] G. Madhusudhan Reddy, K. Satya Prasad, K. S. Rao, T. Mohandas, *Surf Eng.* **27**(2), 92 (2011).
- [9] Hiroshi Tokisue, Kazuyoshi Katoh, Toshikatsu Asahina, Toshio Usiyama, *Deposit. Mater. Trans.*, **47**(3), 874 (2006).
- [10] P. Vilaca, H. Hanninen, T. Saukkonen, R. M. Miranda, *Weld World* **58**, 661 (2014).
- [11] K. Yoshinori, T. Masashi, S. Takeshi, N. Keishi, *Welding in the World* **53**, 272 (2009).
- [12] J. Gandra, D. Pereira, R. M. Miranda, R. J. C. Silva, P. Vilaca, *Surface & coatings Technology* **223**, 32 (2013).
- [13] D. Pereira, J. Gandra, J. Pamies-Teixeira, R. M. Miranda, P. Vilaca, *J. Mater. Process. Technol.* **214**, 2858 (2014).
- [14] R. Puli, G. D. Janaki Ram, *Corrosion Science* **62**, 95 (2012).
- [15] Amit Kumar Singh, G. Madhusudhan Reddy, K. Srinivas Rao, *Defence Technology* **11**(3), 299015).
- [16] D. Govardhan, A. C. S. Kumar, K. G. K. Murthi, G. M. Reddy, *Materials & Design* **36**, 206(2012).
- [17] K. P. Rao, A. Sankar, H. K. Rafi, G. D. Janaki Ram, G. M. Reddy, *Int. J. Adv. Manuf. Technology* **65**, 755 (2013).
- [18] R. Kumar, S. Chattopadhyaya, A. Ghosh, G. M. Krolczyk, P. Vilaca, *Transactions of Famena* **XLI**(2), 61 (2017).
- [19] Stefanie Hanke, Ian Sena, S. Rodrigo Coelho, F. Jorge Dos Santos, *Materials and Manufacturing Processes* **33**(3), 270 (2017).
- [20] R. George Sahaya Nixon, B. S. Mohanty, G. B. Bhaskar, *Materials and Manufacturing Processes* **33**(7), 778 (2017).
- [21] Samuel Silvério, Hennin Krohn, Viktoria Fitseva, Nelson Guedes De Alcântara,

- Jorge Fernandez Dos Santos, *Soldagem & Inspeção* **23**(2), 225 (2018).
- [22] Juan Carlos Galvis, Pedro Henrique Fernandes, Oliveira, Juliana De Paula Martins, André Luis Moreira De Carvalho, *Materials Research* **21**(3), 1 (2018).
- [23] Li Hongjun, Wei Qin, Alexander Galloway, Athanasios Toumpis, *Metals* **9**(479), 2 (2019).
- [24] Seyedeh Marjan Bararpour, Hamed Jamshidi Aval, Roohollah Jamaati, *Journal of alloys and compounds* **805**, 57 (2019).
- [25] H. Khalid Rafi, G. Janaki Ram, G. Phanikumar, *Mater. Sci. Forum* **638**, 864 (2010)
- [26] I. Voutchkov, Jaworski, V. I. Vitanov, G. M. Bedford, *Surf. Coat. Technol.* **141**, 26 (2001).
- [27] B. Muralikrishnan, J. Raja, *Computational Surface and Roundness Metrology*, Springer, London, (2009).